ACS PHYSICAL CHEMISTRY Au
AN OPEN ACCESS JOURNAL OF THE AMERICAN CHEMICAL SOCIETY

pubs.acs.org/physchemau

Article

Mixing Ionic Liquids Affects the Kinetics and Thermodynamics of the Oxygen/Superoxide Redox Couple in the Context of Oxygen Sensing

Jesse W. Mullen, Hua Li, Rob Atkin, and Debbie S. Silvester*

Cite This: *ACS Phys. Chem Au* 2022, 2, 515–526

Read Online

ACCESS | Metrics & More | Article Recommendations | Supporting Information

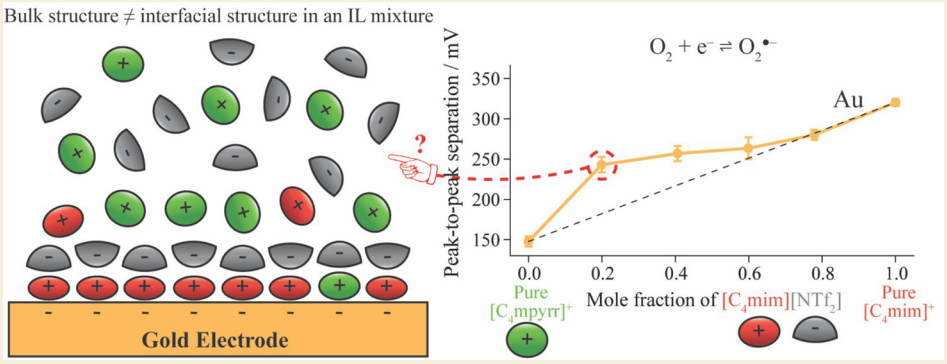

ABSTRACT: The electrochemical oxygen reduction reaction is vital for applications such as fuel cells, metal air batteries and for oxygen gas sensing. Oxygen undergoes a 1-electron reduction process in dry ionic liquids (ILs) to form the electrogenerated superoxide ion that is solvated and stabilized by IL cations. In this work, the oxygen/superoxide ($O_2/O_2^{\bullet-}$) redox couple has been used to understand the effect of mixing ILs with different cations in the context of developing designer electrolytes for oxygen sensing, by employing cyclic voltammetry at both gold and platinum electrodes. Different cations with a range of sizes, geometries and aromatic/aliphatic character were studied with a common bis(trifluoromethylsulfonyl)imide ($[NTf_2]^-$) anion. Diethylmethylsulfonium ($[S_{2,2,1}]^+$), *N*-butyl-*N*-methylpyrrolidinum ($[C_4mpyrr]^+$) and tetradecyltrihexylphosphonium ($[P_{14,6,6,6}]^+$) cations were mixed with a common 1-butyl-3-methylimidazolium ($[C_4mim]^+$) cation at mole fractions (x) of $[C_4mim]^+$ of 0, 0.2, 0.4, 0.6, 0.8, and 1. Both the redox kinetics and thermodynamics were found to be highly dependent on the cation structure and the electrode material used. Large deviations from "ideal" mixtures were observed for mixtures of $[C_4mim][NTf_2]$ with $[C_4mpyrr][NTf_2]$ on gold electrodes, suggesting a much higher amount of $[C_4mim]^+$ ions near the electrode surface despite the large excess of $[C_4mpyrr]^+$ in the bulk. The electrical double layer structure was probed for a mixture of $[C_4mim]_{0.2}[C_4mpyrr]_{0.8}[NTf_2]$ using atomic force microscopy measurements on Au, revealing that the first layer was more like $[C_4mim][NTf_2]$ than $[C_4mpyrr][NTf_2]$. Unusually fast kinetics for $O_2/O_2^{\bullet-}$ in mixtures of $[C_4mim]^+$ with $[P_{14,6,6,6}]^+$ were also observed in the electrochemistry results, which warrants further follow-up studies to elucidate this promising behavior. Overall, it is important to understand the effect on the kinetic and thermodynamic properties of electrochemical reactions when mixing solvents, to aid in the creation of designer electrolytes with favorable properties for their intended application.

KEYWORDS: *ionic liquids, binary mixing, electrochemistry, oxygen reduction, cyclic voltammetry, kinetics, electrical double layer*

1. INTRODUCTION

Room temperature ionic liquids—abbreviated to ionic liquids (ILs) in this work—are defined as liquids entirely composed of ions with melting points below 25 °C.[1] The combination of fluid behavior and purely ionic composition gives ILs intrinsic electrical conductivity, which along with other beneficial properties, including significant electrochemical and thermal stability,[2,3] negligible volatility[2] and chemical tuneability, makes them ideal candidates as electrolytes for various electrochemical applications.[4,5]

The vast number of cation−anion combinations and the ease with which many ion analogues can be synthesized lead to a large number of unique ionic liquids, resulting in them being referred to as "designer solvents".[4,6,7] This number is even

Received: August 7, 2022
Revised: September 17, 2022
Accepted: September 19, 2022
Published: September 26, 2022

https://doi.org/10.1021/acsphyschemau.2c00035
ACS Phys. Chem Au 2022, 2, 515–526

greater when more than one ionic liquid is mixed together to form a mixed IL electrolyte. A high degree of tuneability in the physicochemical[8,9,18−21,10−17] and electrochemical[8,19,20,22−25] properties of IL electrolytes has been demonstrated by "binary mixing", defined as the mixing of two constituent ILs with a common ion. For example, the molar volume and enthalpy of mixtures of hexafluorophosphate ($[PF_6]^-$) and tetrafluoroborate ($[BF_4]^-$) ions with a common 1-butyl-3-methylimidazolium ($[C_4mim]^+$) cation showed a near-linear relationship with increasing mole fraction (x) of $[C_4mim][PF_6]$ in the mixture.[26] Similarly, a linear trend between the logarithm of conductivity and mole fraction of *N*-methyl-*N*-propylpyrrolidinium bis(fluorosulfonyl)imide ($[C_3mpyrr][FSI]$) with the corresponding pyrrolidinium bis(trifluoromethylsulfonyl)imide ($[C_3mpyrr][NTf_2]$) was reported.[9] Evidently, it may be possible to develop task-specific electrolytes by imparting the desirable properties of one IL to a mixture by carefully choosing the IL structures. However, not all IL mixtures follow ideal, linear trends, especially where the mixed ions differ significantly in size.[21] Therefore, more investigations are required to understand the interactions between mixed ILs and why this may result in less predictable changes to the physical and electrochemical properties.

Molecular dynamics (MD) simulations and electrochemical impedance spectroscopy (EIS) techniques have been used to probe the relationship between bulk composition and differential capacitance of binary IL mixtures.[22,23,27,28] This knowledge informs the development of more effective electrical double layer capacitors or supercapacitors. For example, mixtures of tris(pentafluoroethyl)trifluorophosphate ($[FAP]^-$) and $[PF_6]^-$ with a common $[C_4mim]^+$ cation resulted in enhanced capacitance at positive potentials compared to the constituent ILs when the mole fraction of $[C_4mim][PF_6]$ was 0.2.[22] This was attributed to a combination of: (1) the smaller $[PF_6]^-$ anions displacing some of the larger $[FAP]^-$ anions, and (2) filling of the "voids" between $[FAP]^-$ ions with $[PF_6]^-$ ions. This behavior resulted in the formation of a more compressed electrical double layer (EDL), hence increasing the charge density. This demonstrates that the composition of the EDL is modifiable and is linked to the competing interactions of the ions in the mixture, both with each other and with the electrode surface at different applied potentials. Further exploration of these interactions in both the EDL and in the bulk of IL mixtures will aid in developing specialized electrolytes for supercapacitors and other electrochemical applications.

One application where mixed ILs have not yet been investigated in detail is for voltammetric/amperometric sensing. In this context, understanding the kinetics and thermodynamics of a redox reaction of a dissolved species (which we term an "analyte") is integral to developing a robust and fit-for-purpose sensor with a chosen bias potential. The oxygen-superoxide redox couple (eq 1) is known to have highly variable voltammetric behavior in aprotic room temperature ILs,[29−34] making it an ideal analyte for studying changes to the redox kinetics when mixing ILs.

$$O_2 + e^- \rightleftharpoons O_2^{\bullet -} \quad (1)$$

Upon generation, the negatively charged superoxide ($O_2^{\bullet -}$) anion is expected to be solvated by the positively charged IL cation.[35] Cations will be present in at least the first (Stern) layer of the EDL during oxygen reduction upon the application of a negative bias potential,[36,37] so are expected to have the most influence on the electrochemical behavior of the oxygen/superoxide redox couple, as we reported previously.[38] The different voltammetric behavior of the $O_2/O_2^{\bullet -}$ redox couple is exemplified by comparing the behavior of imidazolium cations with tetraalkylphosphonium ($[P_{n,m,m,m}]^+$) cations. The $O_2/O_2^{\bullet -}$ redox couple in $[C_4mim][NTf_2]$ has significantly faster kinetics compared to that in $[P_{14,6,6,6}][NTf_2]$,[32] making $[C_4mim][NTf_2]$ a much more favorable electrolyte for sensing because of the lower applied ('bias') potential required. However, since oxygen gas sensors need to work in a wide range of environments with different humidities, the influence of humidity on the reduction potentials needs to be carefully considered.

We previously demonstrated that the $[P_{14,6,6,6}]^+$ cation resulted in a more stable current response under humidified conditions for the oxygen reduction reaction, compared to smaller cations like $[C_4mim]^+$, because of the large alkyl chains on the phosphonium which exclude water from the electrode−electrolyte interface.[38] The hydrophobic nature of the $[P_{14,6,6,6}]^+$ cation minimized the effect of moisture on the follow-up chemical reactions of superoxide with water (eq 2)[31,34] and effectively prevented further follow-up chemical and electrochemical reactions that typically occur in aqueous-based solvents and other water saturated ILs (eqs 3 and 4).[35,38,39] If mixing the two ILs $[C_4mim][NTf_2]$ and $[P_{14,6,6,6}][NTf_2]$ imparted the desirable qualities of both ILs (i.e., faster kinetics and better hydrophobicity), it may progress toward the development of a sensitive and robust electrolyte for sensing oxygen gas under ambient conditions.

$$2O_2^{\bullet -} + H_2O \rightarrow O_2 + HO_{2^-} + OH^- \quad (2)$$

$$O_2 + 2H^+ + 2e^- \rightarrow H_2O_2 \quad (3)$$

$$O_2 + 4H^+ + 4e^- \rightarrow H_2O \quad (4)$$

The effect of mixing on the macroscopic properties of IL electrolytes is important for informing the development of task-specific electrolytes for a desired application. Yet, the microscopic changes in interactions between ions in the bulk electrolyte and at the electrode interface are the driving force for many of these macroscopic changes. To develop an insightful understanding of the mixing phenomenon on ILs, it is important to consider the relationship between formation of the EDL at the electrolyte−electrode interface and the role of the EDL in larger-scale properties like heterogeneous redox kinetics and redox potentials. In this work, we attempt to address this by using cyclic voltammetry (CV) to investigate the changes to the peak-to-peak separation (ΔE_p) and midpoint potential (E_{mid}) of the $O_2/O_2^{\bullet -}$ redox couple at different IL compositions in binary mixtures of ILs. ΔE_p is used here to represent the redox kinetics because the heterogeneous rate constant (k_0) is inversely proportional to ΔE_p, via a dimensionless kinetic parameter (Υ), as proposed by Nicholson.[40,41] Similarly, the E_{mid} is used to infer the formal potential (E_f^0) of a redox couple under nonstandard conditions.[42] When E_f^0 is subtracted from the applied potential (E_{app}), as presented in the Butler−Volmer expression ($E_{app} - E_f^0$), this is analogous to the activation energy (E_a) in the Arrhenius equation.[43] To rationalize the electrochemical behavior observed in the mixtures, the structure of the electrode−electrolyte interface is also probed for one IL binary mixture using atomic force microscopy (AFM) to examine the physical nature and ion structuring of the EDL.

https://doi.org/10.1021/acsphyschemau.2c00035
ACS Phys. Chem Au 2022, 2, 515−526

2. EXPERIMENTAL SECTION

2.1. Chemical Reagents

All ILs were obtained from commercial suppliers at the highest purity possible. 1-Butyl-3-methylimidazolium bis(trifluoromethylsulfonyl)-imide ($[C_4mim][NTf_2]$, 99.5%, Ionic Liquids Technologies (IoLiTec), Heilbron, Germany), diethylmethylsulfonium bis-(trifluoromethylsulfonyl)imide ($[S_{2,2,1}][NTf_2]$, 99%, IoLiTec), *N*-butyl-*N*-methylpyrrolidinium bis(trifluoromethylsulfonyl)imide ($[C_4mpyrr][NTf_2]$, 99.5%, IoLiTec) , and trihexyltetradecylphosphonium bis(trifluoromethylsulfonyl)imide ($[P_{14,6,6,6}][NTf_2]$, >98%, IoLiTec) were used as received. The chemical structures of the IL anions employed in this work are presented in Figure 1. Ultrapure

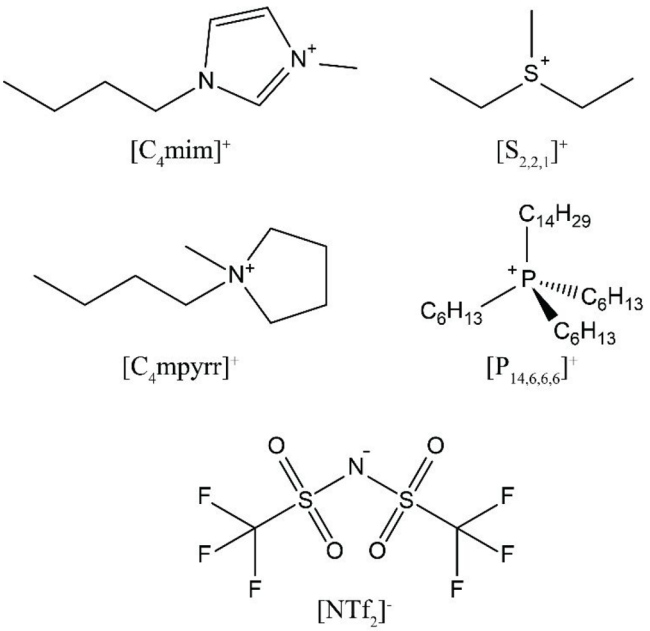

Figure 1. Molecular structures and abbreviations of the IL ions investigated in this work.

water with a resistivity of 18.2 MΩ cm prepared by a Milli-Q laboratory water purification system (Millipore, North Ryde, NSW, Australia) was used for washing thin-film electrodes (TFEs) prior to use. Acetone (for HPLC, ≥99.0%, Chromasolv, Seelze, Germany), acetonitrile (99.8%, Merck, Bayswater, VIC, Australia), ethanol (99%, Merck) and ferrocene (98%, Merck) were used as received. A stock solution of aqueous sulfuric acid (0.5 M) was prepared using ultrapure water from a 95−98 wt % sulfuric acid solution (Ajax Finechem, WA, Australia) and used for the electrochemical activation of the TFEs. High-purity oxygen gas (>99.5%) and high-purity nitrogen gas (>99.99%) were purchased from BOC Gases (Welshpool, WA, Australia).

2.2. Preparation of Binary Mixtures of ILs and Nomenclature Used for Mixtures

Binary mixtures of $[C_4mim][NTf_2]$ with $[S_{2,2,1}][NTf_2]$, $[C_4mpyrr][NTf_2]$ and $[P_{14,6,6,6}][NTf_2]$ were prepared gravimetrically from the pure ILs and mixed thoroughly in a glass vial at room temperature using a stirrer bar at 400 rpm for >20 min prior to each experiment. The following (approximate) compositions were used for the mixtures: $[C_4mim]_{0.8}[Z]_{0.2}[NTf_2]$, $[C_4mim]_{0.6}[Z]_{0.4}[NTf_2]$, $[C_4mim]_{0.4}[Z]_{0.6}[NTf_2]$ and $[C_4mim]_{0.2}[Z]_{0.8}[NTf_2]$. Here, [Z] represents the aliphatic cation in the mixture (either $[S_{2,2,1}]^+$, $[C_4mpyrr]^+$ or $[P_{14,6,6,6}]^+$), and the subscript numbers represent the mole fraction of the cation.

2.3. Electrochemical Experiments

CV measurements were performed using a PGSTAT101 Autolab potentiostat (Metrohm, Gladesville, NSW, Australia) interfaced with a computer with NOVA 2.15 software. All electrochemical experiments were performed inside an aluminum Faraday cage to minimize electromagnetic interference at laboratory room temperature (21 ± 1 °C). The TFEs (MicruX Technologies, Oviedo, Spain) consisted of a 1 mm diameter disk working electrode (WE), a counter electrode (CE), and a reference electrode (RE) deposited on a Pyrex substrate, with all three electrodes consisting of the same metal, either gold or platinum. The TFEs were electrically connected to the potentiostat using a connector made in-house from an IC test clip (Pomona Electronics, Everett, WA, USA) with wires soldered to the gold-plated connections. The WE was electrochemically activated prior to each experiment by CV cycling in a 0.5 M sulfuric acid solution between −0.80 and 0.70 V at 1 V s^{-1} for ca. 200 cycles, or until the CVs converged. The activated electrodes were then washed with ultrapure water and then acetone before drying under a nitrogen stream.

2 μL of the pure IL or the IL mixture was dropcasted to cover all three electrodes on the TFE and purged under a nitrogen stream for ca. 30 min at a flow rate of 1 L min^{-1} to remove dissolved gases and impurities. Once a reproducible blank CV was obtained, pure oxygen gas was introduced into the arm of a modified T-cell, as previously reported by our research group.[44] The flow rate was set to 1 L min^{-1}, and the system was left for 15 min to equilibrate prior to running any CV scans. CV scans were then performed to ensure the gas was properly saturated. If the CV scans were not reproducible after this equilibration time, then the system was given another 10 min to equilibrate and was monitored by CV following this second equilibration period. However, the initial 15 min was typically sufficient to achieve equilibration because of the small volume of electrolyte and high gas flow rate employed. All experiments were repeated at least in triplicate with all data points presented representing the average of the triplicate experiments. The error bars (if presented) represent one standard deviation of the triplicate experiments.

To account for the instability of the gold and platinum quasi-REs on the TFEs, ferrocene (ca. 3 mM) was used as an internal standard so that the potential of the redox couple could be fairly compared across each experiment and between both electrode materials. Fc in acetonitrile (3 mM) was added to the ILs *in situ*, and the acetonitrile was allowed to evaporate. The potential of the CVs for the oxygen reduction reaction was then shifted such that the midpoint of the ferrocene/ferrocenium (Fc/Fc^+) redox couple was at 0 V. This was carried out for all cyclic voltammograms in this work to ensure a fixed and stable reference potential scale.

2.4. Atomic Force Microscopy Experiments

Interfacial normal force measurements were acquired continuously using a Veeco (NY, USA) NanoScope IV Multimode AFM with an EV scanner in contact mode. All experiments were performed at room temperature (21 °C) in a sealed, insulated box to exclude external vibrations and minimize temperature variations. The force profiles presented had a vertical (normal to the surface/electrolyte interface) scan size of 50 nm at a scan rate of 0.2 Hz. The atomically smooth Au(111) surface (a gold film of 300 nm thickness on mica, Georg Albert PVD − Beschichtungen), AFM probe (NSC36, Micromasch, Estonia; cantilever force constant of 0.8 ± 0.1 N m^{-1}) and AFM fluid cell were cleaned with ultrapure water and ethanol, then dried under a nitrogen stream. The Au(111) surface and AFM probe were also cleaned with UV-ozone for 15 min prior to use. A WaveNano potentiostat (Pine Research, NC, USA) was used to measure the open-circuit potential (OCP) and to apply a negative potential (−1 V vs OCP) to the Au(111) surface prior to force profile measurements. All experiments were completed in duplicate on different areas of the surface.

https://doi.org/10.1021/acsphyschemau.2c00035
ACS Phys. Chem Au 2022, 2, 515−526

3. RESULTS AND DISCUSSION

The ILs $[C_4mim][NTf_2]$, $[S_{2,2,1}][NTf_2]$, $[C_4mpyrr][NTf_2]$ and $[P_{14,6,6,6}][NTf_2]$ were selected as solvents to study the voltammetry of the oxygen/superoxide redox couple in the pure ILs and in binary IL mixtures. $[C_4mim]^+$ was chosen as the main cation for all mixtures studied to focus on the effects of mixing an ion with delocalized charge (aromatic) with ions with point charges (aliphatic). The aliphatic series of cations ($[S_{2,2,1}]^+$, $[C_4mpyrr]^+$ and $[P_{14,6,6,6}]^+$) reflect an increase in cation size and amphiphilicity ($[S_{2,2,1}]^+ < [C_4mpyrr]^+ < [P_{14,6,6,6}]^+$). $[NTf_2]^-$ was chosen as a common anion due to its reasonably high hydrophobicity, good chemical and electrochemical stability and its reduced interactions with cations relative to other common IL anions.[11,38] Mole fractions (x) of ca. 0, 0.2, 0.4, 0.6, 0.8, and 1 in the mixtures are explored.

3.1. Electrochemical Experiments

CV was performed on both platinum and gold TFEs to examine the behavior of the oxygen/superoxide ($O_2/O_2^{\bullet-}$) redox couple on different electrode surfaces. It is already well-known that the electrode material can influence the electrochemical windows[45−48] and electrochemical properties of dissolved analytes, and oxygen reduction has been widely characterized on different electrodes in various pure ILs.[30,32,38,49,50]

3.1.1. Voltammetry for Oxygen Reduction in the Pure ILs. CVs for the $O_2/O_2^{\bullet-}$ redox couple on gold and platinum TFEs in the four pure ILs are presented in Figure 2. The peak-to-peak separations (ΔE_p) for the $O_2/O_2^{\bullet-}$ redox couple for both electrode surfaces are given in Table 1, and follow the trend:

$$[C_4mpyrr][NTf_2] < [S_{2,2,1}][NTf_2] < [C_4mim][NTf_2] \ll [P_{14,6,6,6}][NTf_2] \quad (5)$$

This trend suggests that the superoxide radical is reasonably well solvated by the pyrrolidinium and sulfonium cations because of their relatively accessible point charges, whereas the imidazolium cation has a delocalized charge which makes the solvation of superoxide more difficult. The very wide ΔE_p values in the phosphonium IL represent the difficulty for the superoxide to access the positive charge on the central phosphorus atom because it is quite well shielded by the long and flexible carbon chains. Marcus theory predicts that the heterogeneous rate constants will be much slower if there are significant changes in the solvation of the superoxide radical compared to oxygen,[43] which is demonstrated here for the phosphonium IL.

The ΔE_p values obtained in this work are in good agreement with those reported by other groups on conventional macrodisk electrodes (summarized in Table S1 in the Supporting Information).[32,49] We note that different types of electrode surfaces, such as single crystal vs polycrystalline surfaces, can also affect the redox kinetics, in addition to the cleanliness of the electrode,[42] so some degree of variability is expected even with the same electrode material. The voltammetric wave shapes appear to be similar on both electrodes, with a consistently wider ΔE_p on platinum compared to gold. The more "sluggish" kinetics at platinum electrodes is quite well documented for the reduction of oxygen in ILs.[50,51]

A notable feature in the CVs in Figure 2 is the smaller reverse peak for superoxide oxidation in the imidazolium IL compared to the other ILs. This is believed to be caused by the presence of an acidic hydrogen in the C(2) position of the imidazolium ring, which makes $[C_4mim]^+$ more prone to nucleophilic attack by the reactive superoxide species[49] compared to the aliphatic cations, $[C_4mpyrr]^+$, $[S_{2,2,1}]^+$ and $[P_{14,6,6,6}]^+$. Subsequently, the shapes of the CVs for $O_2/O_2^{\bullet-}$ in $[C_4mim][NTf_2]$ are not fully chemically reversible, although they are still reversible enough on the voltammetric time scale to observe a visible superoxide peak. While this chemical reactivity is important to consider, it is not believed to affect

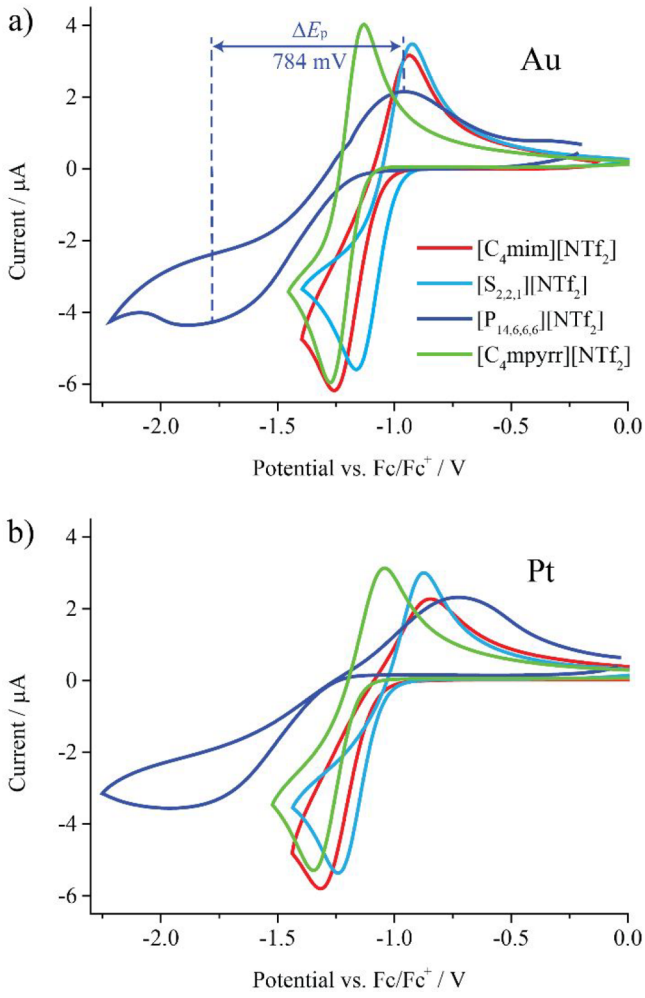

Figure 2. Typical cyclic voltammograms at 100 mVs^{-1} for the $O_2/O_2^{\bullet-}$ redox couple (reduction of saturated oxygen) in the four pure ILs: $[C_4mim][NTf_2]$ (red), $[S_{2,2,1}][NTf_2]$ (blue), $[C_4mpyrr][NTf_2]$ (green) and $[P_{14,6,6,6}][NTf_2]$ (purple) on (a) gold and (b) platinum TFEs.

Table 1. Peak-to-peak separations (ΔE_p) for the $O_2/O_2^{\bullet-}$ redox couple in ILs measured on Au and Pt TFE surfaces at a scan rate of 100 mV s^{-1}

ionic liquid	viscosity[a] (η/cP)	ΔE_p on Au TFE[b] (mV)	ΔE_p on Pt TFE[b] (mV)
$[C_4mim][NTf_2]$	52[3]	320 (±5)	478 (±10)
$[S_{2,2,1}][NTf_2]$	50[52]	240 (±8)	362 (±10)
$[C_4mpyrr][NTf_2]$	89[3]	147 (±6)	317 (±19)
$[P_{14,6,6,6}][NTf_2]$	450[3]	785 (±74)	1049 (±6)

[a]Dynamic viscosity measured at ~293 K and standard pressure (~1 atm). [b]Note: Error bars represent one standard deviation of three repeat measurements.

https://doi.org/10.1021/acsphyschemau.2c00035
ACS Phys. Chem Au 2022, 2, 515−526

the analysis of the electrochemical parameters (peak-to-peak separation and reduction potential) that will be used to draw the conclusions in this study.

3.1.2. Redox Kinetics for Oxygen/Superoxide in $[C_4mim][NTf_2]/[S_{2,2,1}][NTf_2]$ Mixtures. The voltammetry of the $O_2/O_2^{\bullet-}$ redox couple in $[C_4mim]_x[S_{2,2,1}]_{1-x}[NTf_2]$ mixtures at different mole fractions is presented in Figure 3 (Figure 3a on Au, Figure 3b on Pt). On both surfaces, the oxygen reduction peak potential shifts to more negative values as more imidazolium ions are added to the mixture; however, the superoxide oxidation peak potential remains relatively stable. Figure 3c shows quantitively how the ΔE_p values change upon mixing. The values for the pure ILs (mole fractions of 0 and 1) are also included in the plot and are used to draw linear dashed lines that show the expected behavior that represents "ideal" mixing. If the experimental ΔE_p values lie along the dashed line, this indicates that the distribution of ions near the electrode surface (i.e., in the EDL) closely reflects the composition of the mixed ions in the bulk.

As seen in Figure 3c, the ΔE_p values vary on both Au and Pt electrodes with as a higher mole fraction of $[C_4mim]^+$ is added to the mixture. On a gold surface, the behavior approximately follows the ideal mixing line, with some values slightly higher or lower than the ideal mixture. However, on the Pt surface, the experimental ΔE_p values for the mixtures consistently lie below the ideal mixing line, demonstrating kinetics closer to the sulfonium IL than the imidazolium IL. This behavior suggests a higher occupation of sulfonium ions near the Pt electrode surface compared to the bulk. This is rationalized by the negatively biased electrode surface (both Pt and Au) being highly accessible to the charge center of the sulfonium cation due to its trigonal pyramidal geometry, which should result in strong Coulombic interactions between the cation and surface. The geometry allows the $[S_{2,2,1}]^+$ cation to pack quite effectively at the EDL on both Pt and Au, especially compared to more bulkier cations with less accessible charges, cf. pyrrolidinium and phosphonium, which will be discussed later. In contrast, the imidazolium ion is known to have specific adsorption interactions with gold through electrostatic interactions between the metal d-orbital and the π-bonds of the imidazolium ring which causes the ring to lie parallel to the surface.[53−56] Interactions of imidazolium cations are less well-known on a Pt surface; hence, the interactions of Pt with $[S_{2,2,1}]^+$ will likely be stronger than with $[C_4mim]^+$. Overall, the mixtures on Au more closely resemble the ideal bulk composition, representing a balance in the strong interactions of the two ions (sulfonium and imidazolium) with the surface. However, on Pt, slightly more sulfonium ions are likely to be present in the EDL compared to the bulk.

3.1.3. Redox Kinetics for Oxygen/Superoxide in $[C_4mim][NTf_2]/[C_4mpyrr][NTf_2]$ Mixtures. Cyclic voltammetry for the $O_2/O_2^{\bullet-}$ redox couple in $[C_4mim]_x[C_4mpyrr]_{1-x}[NTf_2]$ mixtures at different mole fractions is presented in Figure 4 (Figure 4a on Au, Figure 4b on Pt). Upon visual inspection, the CV behavior and waveshapes on Au (Figure 4a) appear to be closer to that of the pure imidazolium IL for all the mixtures studied. However, on Pt (Figure 4b), there is a more gradual change in the superoxide oxidation peak potential with changing composition. The peak-to-peak separations (ΔE_p) are plotted for the pure ILs and the different mixtures in Figure 4c as a function of increasing mole fraction of $[C_4mim]^+$ in the mixture, with the dashed line representing the "ideal" mixture values. On Pt, the

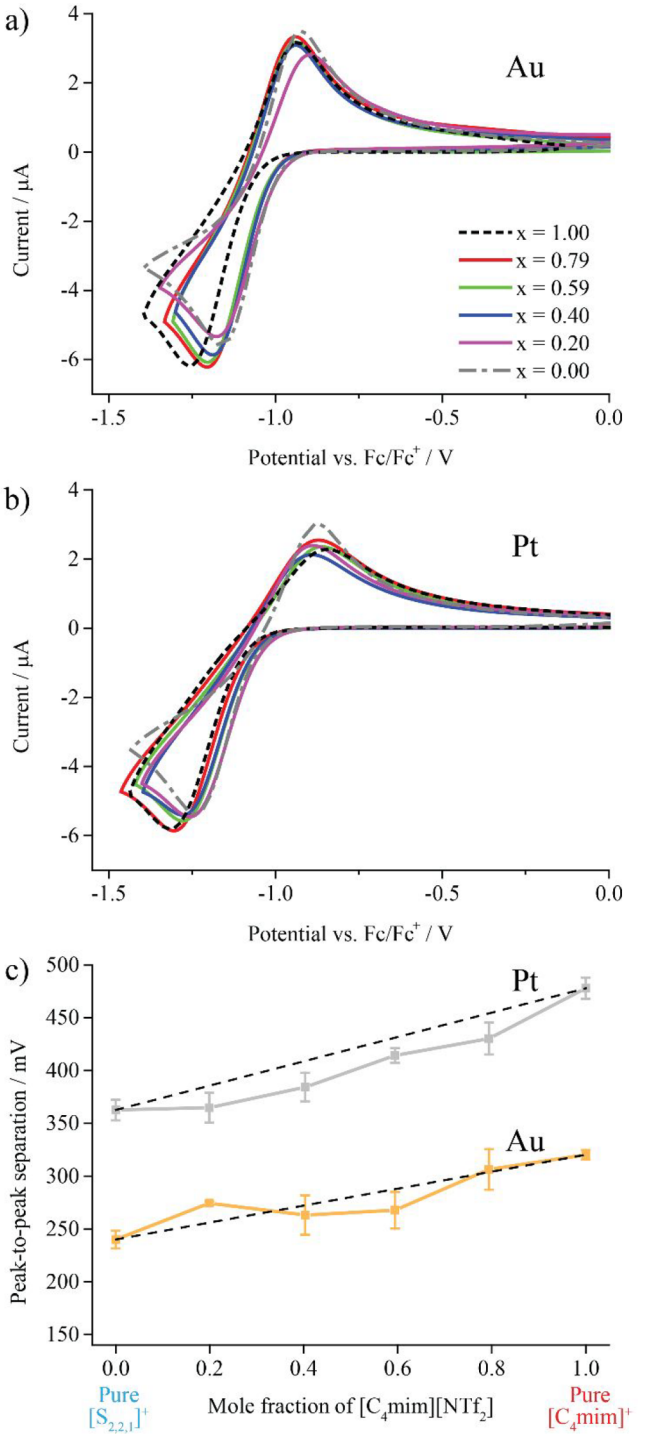

Figure 3. CVs for the $O_2/O_2^{\bullet-}$ redox couple in $[C_4mim]_x[S_{2,2,1}]_{1-x}[NTf_2]$ mixtures (red, green, blue and pink solid lines) with the neat ILs overlaid ($[C_4mim][NTf_2]$, black dashed line; $[S_{2,2,1}][NTf_2]$, gray dashed line) at (a) gold and (b) platinum TFEs. The average ΔE_p for each IL and IL mixture is presented in (c) for both electrode materials (platinum, gray squares; gold, yellow squares). The error bars represent one standard deviation of triplicate experiments. The linear function representing a weighted average of the ΔE_p of the two neat ILs (black dashed line in (c)) is included for clarity. See Table S2 in the Supporting Information for the quantitative data extracted from the plots.

change in the kinetics approximately follows the ideal line, suggesting that the EDL comprises of similar compositions of

https://doi.org/10.1021/acsphyschemau.2c00035
ACS Phys. Chem Au 2022, 2, 515−526

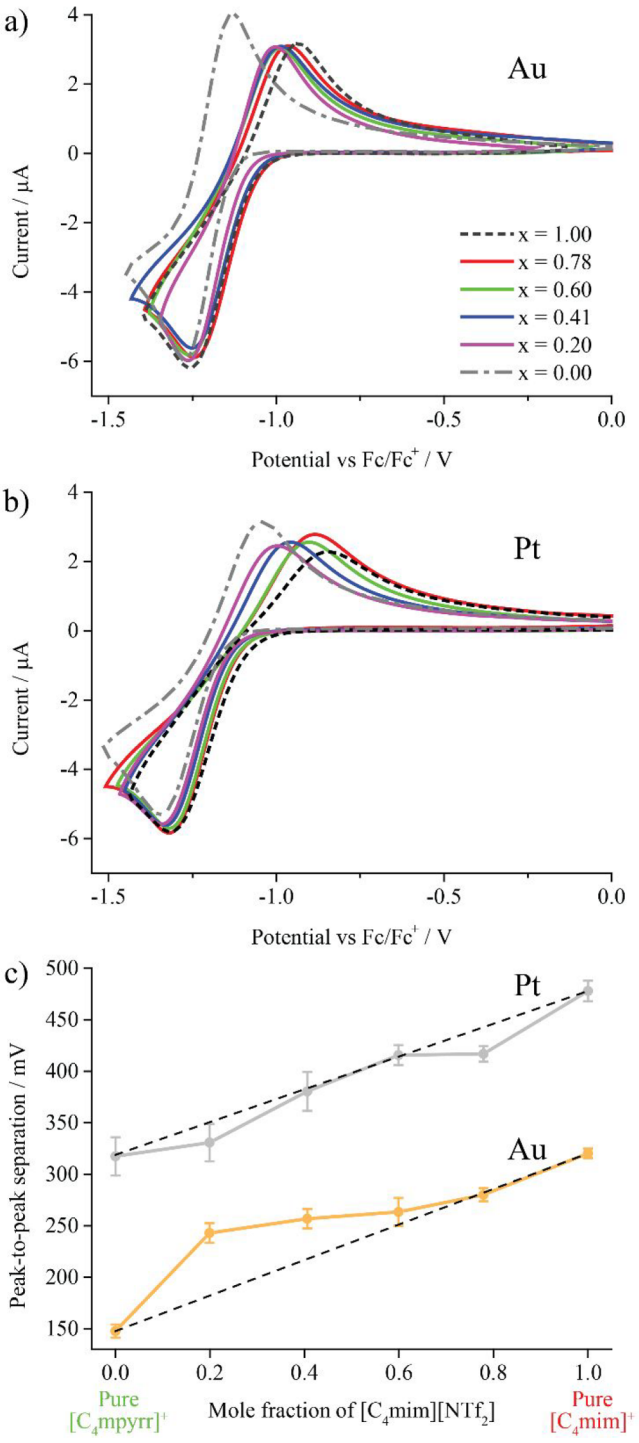

Figure 4. CVs of the $O_2/O_2^{\bullet-}$ redox couple in $[C_4mim]_x[C_4mpyrr]_{1-x}[NTf_2]$ mixtures (red, green, blue and pink solid lines) with the neat ILs overlaid ($[C_4mim][NTf_2]$, black dashed line; $[C_4mpyrr][NTf_2]$, gray dashed line) at (a) gold and (b) platinum TFEs. The average ΔE_p for each IL and IL mixture is presented in (c) for both electrode materials (platinum, gray circles; gold, yellow circles). The error bars represent one standard deviation of triplicate experiments. The linear function representing a weighted average of the ΔE_p of the two neat ILs (black dashed line in (c)) is included for clarity. See Table S3 in the Supporting Information for the quantitative data extracted from the plots.

ions as in the bulk. However, the behavior on Au significantly deviates from ideal, especially at lower mole fractions of $[C_4mim]^+$. For example, at $x = 0.2$, the ΔE_p was >60 mV higher than the "ideal" mixture of the constituent ILs, suggesting that the redox kinetics are much more like pure $[C_4mim][NTf_2]$ than $[C_4mpyrr][NTf_2]$, despite containing four times the number of pyrrolidinium cations in the bulk mixture. This suggests that the cation layers at the interface are likely composed mostly of $[C_4mim]^+$, despite the disproportionate amount of $[C_4mpyrr]^+$ in the bulk.

As mentioned for the $[C_4mim]_x[S_{2,2,1}]_{1-x}[NTf_2]$ mixtures, imidazolium cations are known to have strong interactions with gold surfaces.[53−56] However, for pyrrolidinium cations, contrary findings on the extent of specific adsorption have been reported. X-ray photoelectron spectroscopy of ultrathin IL layers on a Au(111) surface demonstrated that for both $[C_1mim][NTf_2]$ and $[C_8mim][NTf_2]$, the imidazolium cation was oriented parallel to the interface, while the pyrrolidinium cation of $[C_4mpyrr][NTf_2]$ was likely oriented perpendicular to the interface with the alkyl chain pointing away from the surface.[57,58] Based on this, it would be expected that imidazolium cations have stronger electrostatic interactions with the surface because the delocalized charge should be drawn closer to the surface than the point charge of pyrrolidinium. In contrast, the innermost layer of the $[C_4mpyrr][NTf_2]$/Au(111) interface when investigated by AFM was more compact and required higher rupture forces to puncture than the corresponding layer of the $[C_2mim][NTf_2]$/Au(111) interfacial structure.[59] The authors concluded that the localized charge of the pyrrolidinium cation accounted for stronger electrostatic interactions with the gold surface, resulting in the higher rupture forces and a more condensed structure.

While the electrochemical results can give some indications on the structuring at the interface, it is important to note that the composition of the innermost (Stern) layer at the interface may not fully define the redox kinetics. This is because the electron tunnelling distance between an analyte and the electrode surface is likely to be on the order of several nm,[43,60] which is significantly larger than the size of an individual IL ion. Consequently, the height and composition of the entire EDL is likely to be multiple ion layers thick and the combination of these layers could account for changes in the redox kinetics. Previous research found that the $[C_2mim][NTf_2]$/Au(111) interfacial structure was shorter (2.8 nm) than that of $[C_4mpyrr][NTf_2]$/Au(111) (3.8 nm),[59] which may suggest that the negative surface charge of gold is screened more effectively by the more compact EDL of $[C_2mim][NTf_2]$ at the gold interface. Given the complex nature of the factors determining the structure of the interface between ILs and metal electrodes, investigation of the interfacial structure of $[C_4mim]_{0.2}[C_4mpyrr]_{0.8}[NTf_2]$/Au(111) by AFM will be performed later (see section 3.2) to investigate the significant deviation from "ideal" redox kinetics in this mixture suggested from the CV.

3.1.4. Redox Kinetics for Oxygen/Superoxide in $[C_4mim][NTf_2]/[P_{14,6,6,6}][NTf_2]$ Mixtures. The voltammetry of the $O_2/O_2^{\bullet-}$ redox couple in $[C_4mim]_x[P_{14,6,6,6}]_{1-x}[NTf_2]$ mixtures at different mole fractions is presented in Figure 5 (Figure 5a on Au, Figure 5b on Pt). This mixture demonstrated the greatest deviation from "ideal" and showed different characteristics to those observed for the other mixtures. We note that unusual electrochemical behavior in ILs with the $[P_{14,6,6,6}]^+$ cation has been observed by our research group previously.[61,62] The voltammetric wave shapes

https://doi.org/10.1021/acsphyschemau.2c00035
ACS Phys. Chem Au 2022, 2, 515−526

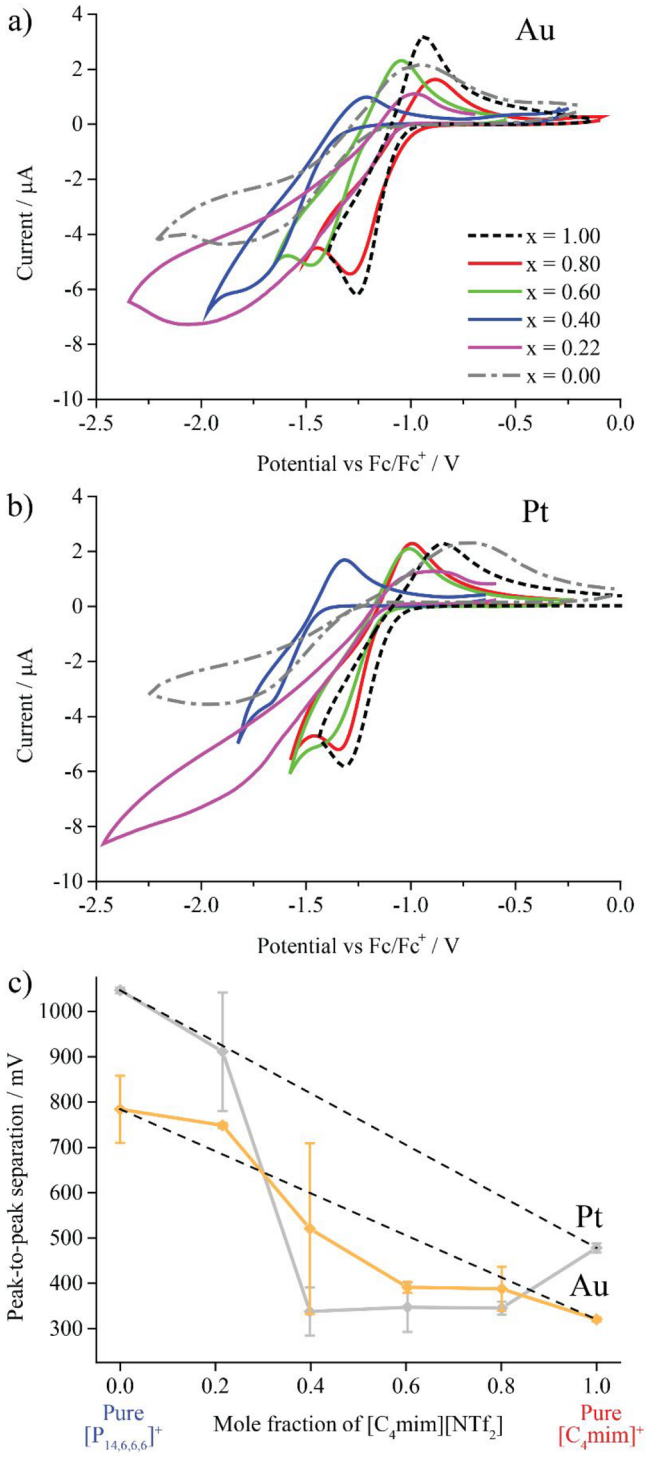

Figure 5. CVs of the $O_2/O_2^{\bullet-}$ redox couple in $[C_4mim]_x[P_{14,6,6,6}]_{1-x}[NTf_2]$ mixtures (red, green, blue and pink solid lines) with the neat ILs overlaid ($[C_4mim][NTf_2]$, black dashed line; $[P_{14,6,6,6}][NTf_2]$, gray dashed line) at (a) gold and (b) platinum TFEs. The average ΔE_p for each IL and IL mixture is presented in (c) for both electrode materials (platinum, gray circles; gold, yellow circles). The error bars represent one standard deviation of triplicate experiments. The linear function representing a weighted average of the ΔE_p of the two neat ILs (black dashed line in (c)) is included for clarity. See Table S4 in the Supporting Information for the quantitative data extracted from the plots.

on both Au and Pt surfaces changed significantly as $[C_4mim]^+$ was added to the mixture. Notably, at some mixtures (e.g., x = 0.22), the appearance of two reduction peaks were observed intermittently (see discussion in the Supporting Information), which could correspond to the reductions of the oxygen and superoxide, respectively;[33] however, the behavior is unclear and often inconsistent. In this case, the best estimate was made by measuring the peak potentials using a peak that was clearly visible. It is noted that the broader nature of the peak at high $[P_{14,6,6,6}]^+$ compositions also makes measurement of the peak potentials more prone to errors.

Figure 5c shows how the peak-to-peak separations change with increasing mole fraction in the mixture. On Au, ΔE_p roughly follows the ideal mixing line, with a slight tendency for the kinetics to be closer to pure $[C_4mim][NTf_2]$ at mole fractions from 0.4 to 0.8. We note that the value for x = 0.2 may be skewed because of the split peak nature of the CV and the difficulty to measure an accurate ΔE_p. The trend on Au is similar to that reported for the other mixtures, with stronger specific adsorption of $[C_4mim]^+$ at the gold surface compared to the phosphonium cation. However, the behavior on the Pt electrode is very unexpected, because the kinetics actually appear much faster in the mixture (at x = 0.4, 0.6 and 0.8) than in pure $[C_4mim][NTf_2]$ (320 mV) or pure $[P_{14,6,6,6}][NTf_2]$ (784 mV). It is noted that these experiments were highly reproducible and repeated multiple times with the same results. Although the reason for this behavior is not clear, the decrease in ΔE_p of $[C_4mim]_x[P_{14,6,6,6}]_{1-x}[NTf_2]$ mixtures compared to pure $[C_4mim][NTf_2]$ could be a promising step toward developing an oxygen sensing electrolyte with favorable kinetics, but one that is more robust against atmospheric humidity. Further follow-up studies with these mixtures are planned in the future to elucidate the unusual behavior occurring.

3.1.5. Thermodynamic Reduction Potentials for Oxygen/Superoxide in IL Mixtures. The midpoint potentials (E_{mid}) of the $O_2/O_2^{\bullet-}$ redox couple were calculated from the average of the oxygen reduction potential and superoxide oxidation potential. E_{mid} was used rather than the reduction peak potential to account for the widely different kinetics of the redox couple in the different ILs. The potentials were measured relative to the ferrocene/ferrocene redox couple, as described in the Experimental Section, because the quasi-reference electrode potential on the TFE surface may shift during experiments. Ferrocene is often used for reference potential calibration in ILs.[63,64] Figure 6 shows the plots of E_{mid} as a function of increasing mole fraction of $[C_4mim]^+$ (x) in mixtures with (a) $[S_{2,2,1}]^+$, (b) $[C_4mpyrr]^+$ and (c) $[P_{14,6,6,6}]^+$ cations. For the sulfonium mixture (Figure 6a), the midpoint potentials are relatively similar in the pure ILs, with a difference of only ~20 mV on Pt and ~60 mV on Au between pure $[C_4mim][NTf_2]$ and pure $[S_{2,2,1}][NTf_2]$. So, while the E_{mid} at different mole fractions looks quite variable in Figure 6a, these differences are relatively small compared to the other mixtures. Generally, the trends appear to be relatively linear (taking into account the error bars), with a slight tendency toward more $[S_{2,2,1}]^+$ character on the gold and more $[C_4mim]^+$ character on Pt, consistent with the discussion for ΔE_p in Figure 3.

For the $[C_4mim]_x[C_4mpyrr]_{1-x}[NTf_2]$ mixtures (Figure 6b), the E_{mid} potentials of the pure ILs vary by ~110 mV on Pt and ~100 mV on Au. With more $[C_4mim]^+$ in the mixture, E_{mid} decreases closer to the value in the pure $[C_4mim][NTf_2]$.

https://doi.org/10.1021/acsphyschemau.2c00035
ACS Phys. Chem Au 2022, 2, 515−526

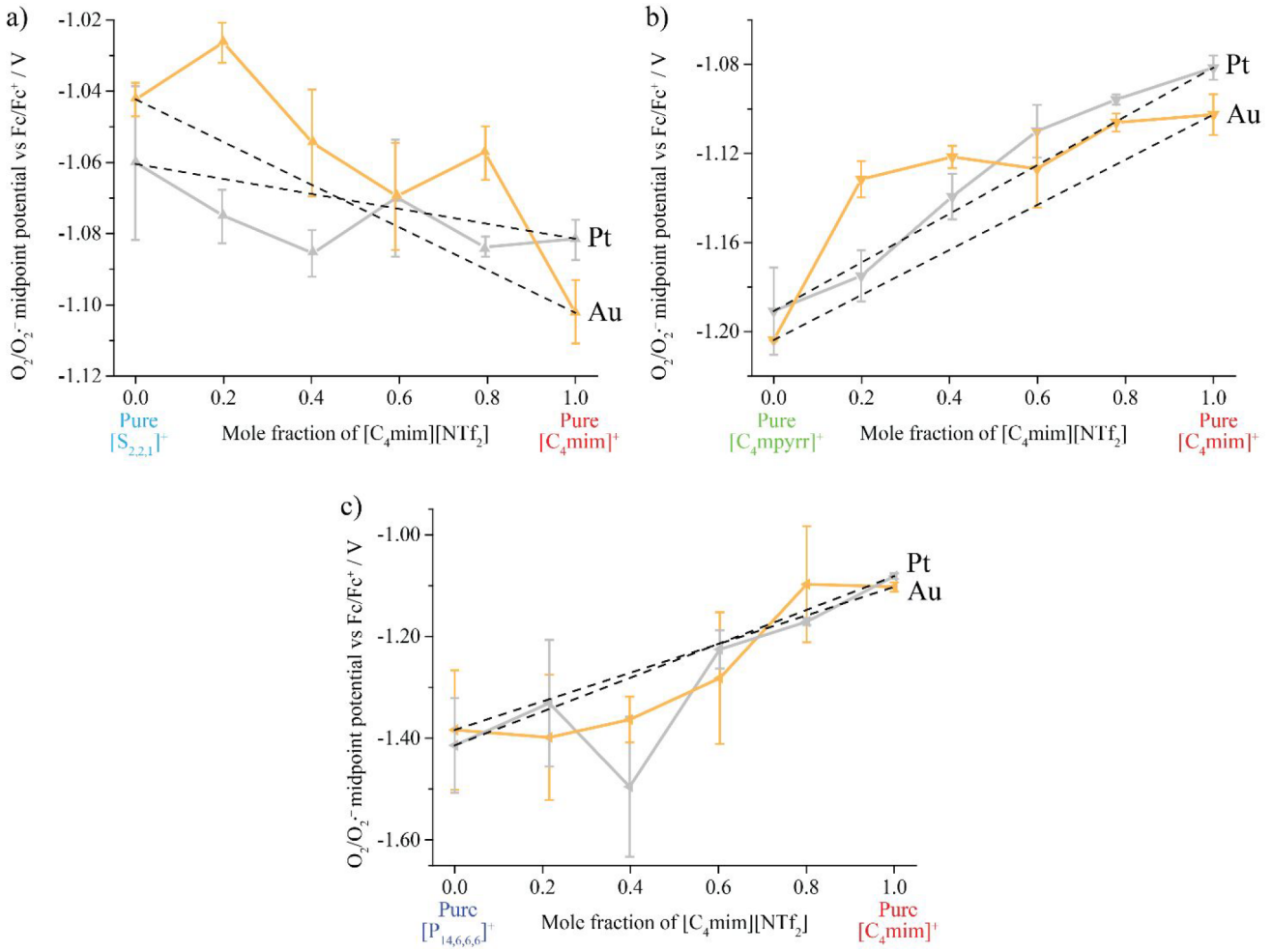

Figure 6. Midpoint potential (E_{mid}) of the $O_2/O_2^{\bullet-}$ redox couple as a function of the mole fraction of $[C_4mim][NTf_2]$ for IL mixtures of $[C_4mim][NTf_2]$ with (a) $[S_{2,2,1}][NTf_2]$, (b) $[C_4mpyrr][NTf_2]$ and (c) $[P_{14,6,6,6}][NTf_2]$. The data for a platinum and gold TFE are presented in gray and yellow, respectively. The error bars represent one standard deviation of triplicate experiments. The linear function representing a weighted average of the E_{mid} for the two pure ILs (black dashed line) is also included for clarity. See Tables S2−S4 in the Supporting Information for the quantitative data.

On the Pt surface, the trend almost follows the "ideal" mixing line (within experimental variation), but on Au, there is a significantly higher character of $[C_4mim][NTf_2]$ even at low mole fractions of $[C_4mim]^+$. This is entirely consistent with the results in Figure 4, where it was suggested that the strong interactions of Au with $[C_4mim]^+$ causes a much higher occupation of $[C_4mim]^+$ near the surface even with a high excess of $[C_4mpyrr]^+$ in the bulk. This mixture will be studied using AFM force curves to try to elucidate the behavior occurring by relating it to the ion structuring at the electrode.

The E_{mid} potentials measured in $[C_4mim]_x[P_{14.6.6.6}]_{1-x}[NTf_2]$ mixtures are shown in Figure 6c. This mixture showed the largest differences in thermodynamics between the two pure ILs, with a difference in E_{mid} of ~330 mV on Pt and ~280 on Au. The trend in E_{mid} with varying mole fraction almost follows the "ideal" line on Pt, except for the outlier at x = 0.4 that shows a much more negative reduction potential than expected. The large error bars represent the inconsistency in results observed for this mixture, probably due to the large and bulky chains of the $[P_{14,6,6,6}]^+$ cation forming different structures in the EDL each time a negative bias is applied. Large and bulky amphiphilic ions such as $[P_{14,6,6,6}]^+$ can induce self-assembly through solvophobic interactions, resulting in quite ordered nanostructures at charged surfaces,[65] whereas $[C_4mim]^+$ cations lie mostly parallel to a gold/platinum surfaces,[27,53,66,67] forming alternating layers of cations-anions-cations-anions, with some "overscreening" of the electrode charge.[68] When more $[P_{14,6,6,6}]^+$ cations are present in the bulk (x < 0.50), there may be a transition from an EDL with the typical alternating layers of ions, to an interfacial structure with alternating layers driven by nanosegregration. However, the presence of $[C_4mim]^+$ in the EDL might influence this transition because the butyl chain can interact with the apolar domain in $[P_{14,6,6,6}]^+$, exhibiting a structure between fully dispersed and fully continuous microphases.[69] The transitional structure may result in competition between the development of the interfacial nanostructure and the noncovalent interactions of phosphonium cations with superoxide (previously discussed) which could result in a higher thermodynamic energy barrier to electron transfer and inconsistencies in double layer formation. However, the exact cause of the E_{mid} vs x behavior is hard to discern through electrochemical means alone and would benefit from simulation data and more insights into the interfacial structure of the $[C_4mim]_x[P_{14,6,6,6}]_{1-x}[NTf_2]$ mixtures at these applied potentials.

https://doi.org/10.1021/acsphyschemau.2c00035
ACS Phys. Chem Au 2022, 2, 515−526

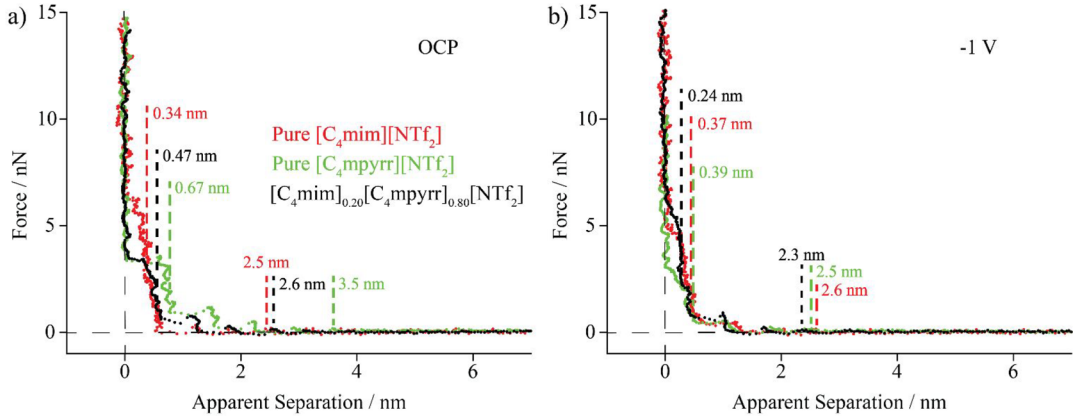

Figure 7. AFM measurements of normal force vs separation of the electrolyte-Au(111) interface for pure $[C_4mim][NTf_2]$ (red), pure $[C_4mpyrr][NTf_2]$ (green) and the mixture $[C_4mim]_{0.20}[C_4mpyrr]_{0.80}[NTf_2]$ (black) at (a) the OCP and (b) −1 V vs the OCP. The force−separation profiles represent a typical profile for each liquid and potential and only show the approach of the AFM probe to the surface for clarity. Widths of the interfacial structure layers are indicated using dashed lines.

3.2. Atomic Force Microscopy of the $[C_4mim]_{0.2}[C_4mpyrr]_{0.8}[NTf_2]$/Au(111) Interface

Based on the electrochemistry results that showed the most obvious deviations from "ideal" mixing, the IL mixture $[C_4mim]_{0.2}[C_4mpyrr]_{0.8}[NTf_2]$ was chosen for further analysis of its interfacial structure by AFM at a gold surface. The force−separation profiles for this mixture, and for the two pure ILs, at a Au(111) interface are presented in Figure 7a at the OCP and in Figure 7b at a bias potential of −1 V. It is noted that the innermost layers of all force−separation profiles measured by AFM typically showed nonvertical steps, indicating that these layers are slightly compressible. Widths are estimated by taking the width measurement at the force value halfway along the step, i.e., the median force value of the compressible layer. As indicated by the dashed lines in Figure 7a, the interfacial structure of the mixture demonstrated characteristic features of both the constituent ILs at the OCP, while under a negative bias potential of −1 V (Figure 7b), the structure of the mixture contained more unique features compared to the pure ILs.

At the OCP, the innermost layer of the mixture had a width of 0.47 nm, between that of the corresponding layers of neat $[C_4mim][NTf_2]$ (0.34 nm) and neat $[C_4mpyrr][NTf_2]$ (0.67 nm). This indicated that the layer closest to the interface may be enriched with $[C_4mim]^+$ in the mixture despite being much less prevalent in the bulk liquid. The length of the interfacial structure measurable by AFM for $[C_4mim]_{0.2}[C_4mpyrr]_{0.8}[NTf_2]$ was 2.6 nm, which was almost identical to the length measured for pure $[C_4mim][NTf_2]$ (2.5 nm) and much less than that shown for pure $[C_4mpyrr][NTf_2]$ (3.5 nm). The values for the pure ILs closely match those previously reported for $[C_2mim][NTf_2]$ and $[C_4mpyrr][NTf_2]$ on a Au(111) surface.[59] However, the force required to rupture the innermost layers of the mixture and pure $[C_4mpyrr][NTf_2]$ was almost identical at 3.4 nN and 3.6 nN, respectively. The lower rupture force relative to $[C_4mim][NTf_2]$ indicates that this innermost ion layer is less tightly bound in the mixture due to competing interactions introduced because of the presence of two different cations. With no applied potential across the interface, the interfacial structure of the mixture $[C_4mim]_{0.2}[C_4mpyrr]_{0.8}[NTf_2]$ appears as an intermediate between the two constituent ILs, possessing characteristics in the force−separation profiles of both ILs despite significant differences in the concentration of the mixed cations.

Under a negative applied potential of −1 V, similar to the midpoint potential for $O_2/O_2^{\bullet-}$ at a gold electrode in Figure 3b, the interface for this mixture demonstrates characteristics unlike the constituent ILs, which likely contributes to the nonideal kinetic and thermodynamic behavior observed. The innermost layer of the interface for the pure ILs was slightly wider and required less force to be penetrated than that of the mixture. Furthermore, the EDL structure for the mixture extended a somewhat shorter distance from the interface (2.3 nm) compared to $[C_4mim][NTf_2]$ (2.6 nm) and $[C_4mpyrr][NTf_2]$ (2.5 nm). Recalling that the ΔE_p of the electrolytes follows the trend:

$$[C_4mpyrr][NTf_2] < [C_4mim]_{0.20}[C_4mpyrr]_{0.80}[NTf_2] < [C_4mim][NTf_2] \quad (6)$$

Comparing the redox kinetics of the pure ILs with characteristics of their respective force−separation profiles suggests that the ΔE_p of an mixed IL electrolyte should decrease with shorter EDL structures and with smaller rupture forces for ion layers closest to the interface ($[C_4mpyrr][NTf_2]$, 3.3 nN; $[C_4mim][NTf_2]$, 5.1 nN). Consequently, the shorter EDL structure observed for the mixture should result in faster kinetics than the neat ILs because the electron tunnelling occurring during a redox reaction transverses a smaller ordered, dense structure. In contrast, the greater rupture forces shown for the inner layers of the EDL in the mixture (6.1 nN) compared to the pure ILs would cause slower kinetics because the electrons must tunnel through a more ordered structure to reach the electrode surface. The two rigidly adhered layers closest to the interface of the mixture appear to offset much of the faster kinetics that would be expected of the mixture because of its much shorter interfacial structure. In summary, the force−separation profiles for the examined ILs and IL mixture demonstrate that the higher rupture force observed in the innermost layers of the mixture, relative to the pure ILs, may account for the slower than "ideal" kinetics observed for $O_2/O_2^{\bullet-}$ in this mixture despite it having a more compact structure normal to the interface.

https://doi.org/10.1021/acsphyschemau.2c00035
ACS Phys. Chem Au 2022, 2, 515−526

4. CONCLUSIONS

Cyclic voltammetry of the $O_2/O_2^{\bullet-}$ redox couple in mixtures of ILs was used to evaluate the redox kinetics and thermodynamics, using the peak-to-peak separation (ΔE_p) and the midpoint potential (E_{mid}), respectively. Three different mixtures were examined, $[C_4mim]_x[S_{2,2,1}]_{1-x}[NTf_2]$, $[C_4mim]_x[C_4mpyrr]_{1-x}[NTf_2]$ and $[C_4mim]_x[P_{14,6,6,6}]_{1-x}[NTf_2]$, on both gold and platinum electrodes. The behavior of the mixtures was found to be dependent on the constituent ILs and the nature of the metal (Au or Pt) at the electrode−electrolyte interface. Factors including ion geometry, specific adsorption interactions between ions and metals and interfacial nanostructuring were found to influence the prevalence of the mixed ions in the EDL and the resulting redox kinetics or thermodynamics. The strong imidazolium-like characteristics in pyrrolidinium-imidazolium mixtures at low imidazolium mole fractions was supported by AFM results that showed a much higher proportion of $[C_4mim]^+$ compared to $[C_4mpyrr]^+$ near the electrode surface. The behavior in the phosphonium mixtures warrants follow-up studies to investigate the behavior occurring. Overall, understanding the effects of mixing ILs on the electrochemical properties of dissolved analytes is important and can aid in developing the optimum electrolyte material for electrochemical sensing and other electrochemical applications.

■ ASSOCIATED CONTENT

Supporting Information

The Supporting Information is available free of charge at https://pubs.acs.org/doi/10.1021/acsphyschemau.2c00035.

Tables of peak-to-peak separations on Au and Pt electrodes in the pure ILs in this work compared to previous literature. Tables of peak-to-peak separations and midpoint potential for $O_2|O_2^{\bullet-}$ in $[C_4mim]_x[S_{2,2,1}]_{1-x}[NTf_2]$, $[C_4mim]_x[C_4mpyrr]_{1-x}[NTf_2]$ and $[C_4mim]_x[P_{14,6,6,6}]_{1-x}[NTf_2]$ mixtures. Example cyclic voltammograms demonstrating the inconsistent peak behavior observed for $[C_4mim]_{0.4}[P_{14,6,6,6}]_{0.6}[NTf_2]$ mixtures on a Au electrode (PDF)

■ AUTHOR INFORMATION

Corresponding Author

Debbie S. Silvester − *School of Molecular and Life Sciences, Curtin University, Perth, Western Australia 6845, Australia;* orcid.org/0000-0002-7678-7482; Phone: +61-08-9266-7148; Email: d.silvester-dean@curtin.edu.au; Fax: +61-08-9266-2300

Authors

Jesse W. Mullen − *School of Molecular and Life Sciences, Curtin University, Perth, Western Australia 6845, Australia;* orcid.org/0000-0002-8998-7977

Hua Li − *School of Molecular Sciences, The University of Western Australia, Perth, Western Australia 6009, Australia; Centre for Microscopy, Characterisation and Analysis, The University of Western Australia, Perth, Western Australia 6009, Australia;* orcid.org/0000-0003-2057-2762

Rob Atkin − *School of Molecular Sciences, The University of Western Australia, Perth, Western Australia 6009, Australia;* orcid.org/0000-0001-8781-7854

Complete contact information is available at: https://pubs.acs.org/10.1021/acsphyschemau.2c00035

Author Contributions

CRediT: **Jesse W. Mullen** conceptualization (equal), data curation (equal), formal analysis (equal), investigation (equal), methodology (equal), writing-original draft (equal), writing-review & editing (equal); **Hua Li** formal analysis (equal), methodology (equal), supervision (equal), writing-review & editing (equal); **Rob Atkin** funding acquisition (equal), resources (equal); **Debbie S. Silvester** formal analysis (equal), funding acquisition (equal), project administration (equal), resources (equal), supervision (equal), writing-original draft (equal), writing-review & editing (equal).

Notes

The authors declare no competing financial interest.

■ ACKNOWLEDGMENTS

The authors acknowledge the ARC for funding through a Discovery Project (DP210102119). D.S.S. thanks the Australian Research Council (ARC) for funding through a Future Fellowship (FT170100315). J.W.M. thanks Curtin University for a Ph.D. scholarship.

■ REFERENCES

(1) MacFarlane, D.; Kar, M.; Pringle, J. *Fundamentals of Ionic Liquids*, 2nd ed; Wiley: Weinheim, Germany, 2017.

(2) Marsh, K. N.; Boxall, J. A.; Lichtenthaler, R. Room temperature ionic liquids and their mixtures - A review. *Fluid Phase Equilib.* **2004**, *219*, 93−98.

(3) Barrosse-Antle, L. E.; Bond, A.; Compton, R. G.; O'Mahony, A. M.; Rogers, E. I.; Silvester, D. S. Voltammetry in room temperature ionic liquids: Comparisons and contrasts with conventional electrochemical solvents. *Chem. - An Asian J.* **2010**, *5*, 202−230.

(4) Welton, T. Ionic liquids: a brief history. *Biophys. Rev.* **2018**, *10*, 691−706.

(5) Silvester, D. S.; Jamil, R.; Doblinger, S.; Zhang, Y.; Atkin, R.; Li, H. Electrical Double Layer Structure in Ionic Liquids and Its Importance for Supercapacitor, Battery, Sensing, and Lubrication Applications. *J. Phys. Chem. C* **2021**, *125*, 13707−13720.

(6) Visser, A. E.; Swatloski, R. P.; Reichert, W. M.; Mayton, R.; Sheff, S.; Wierzbicki, A.; Davis, J. H.; Rogers, R. D. Task-specific ionic liquids for the extraction of metal ions from aqueous solutions. *Chem. Commun.* **2001**, *1*, 135−136.

(7) Freemantle, M. Designer solvents. *Chem. Eng. News Arch* **1998**, *76*, 32−37.

(8) Clough, M. T.; Crick, C. R.; Grasvik, J.; Hunt, P. A.; Niedermeyer, H.; Welton, T.; Whitaker, O. P. A physicochemical investigation of ionic liquid mixtures. *Chem. Sci.* **2015**, *6*, 1101−1114.

(9) Bayley, P. M.; Best, A. S.; MacFarlane, D. R.; Forsyth, M. Transport properties and phase behaviour in binary and ternary ionic liquid electrolyte systems of interest in lithium batteries. *ChemPhysChem* **2011**, *12*, 823−827.

(10) Finotello, A.; Bara, J. E.; Narayan, S.; Camper, D.; Noble, R. D. Ideal gas solubilities and solubility selectivities in a binary mixture of room-temperature ionic liquids. *J. Phys. Chem. B* **2008**, *112*, 2335−2339.

(11) Fox, E. T.; Weaver, J. E. F.; Henderson, W. A. Tuning binary ionic liquid mixtures: Linking alkyl chain length to phase behavior and ionic conductivity. *J. Phys. Chem. C* **2012**, *116*, 5270−5274.

(12) Montanino, M.; Moreno, M.; Alessandrini, F.; Appetecchi, G. B.; Passerini, S.; Zhou, Q.; Henderson, W. A. Physical and

electrochemical properties of binary ionic liquid mixtures: (1 - x) PYR 14TFSI-(x) PYR 14IM 14. *Electrochim. Acta* **2012**, *60*, 163−169.
(13) Podgoršek, A.; Jacquemin, J.; Pádua, A. A. H.; Costa Gomes, M. F. Mixing Enthalpy for Binary Mixtures Containing Ionic Liquids. *Chem. Rev.* **2016**, *116*, 6075−6106.
(14) Matthews, R. P.; Villar-Garcia, I. J.; Weber, C. C.; Griffith, J.; Cameron, F.; Hallett, J. P.; Hunt, P. A.; Welton, T. A structural investigation of ionic liquid mixtures. *Phys. Chem. Chem. Phys.* **2016**, *18*, 8608−8624.
(15) Brooks, N. J.; Castiglione, F.; Doherty, C. M.; Dolan, A.; Hill, A. J.; Hunt, P. A.; Matthews, R. P.; Mauri, M.; Mele, A.; Simonutti, R.; Villar-Garcia, I. J.; Weber, C. C.; Welton, T. Linking the structures, free volumes, and properties of ionic liquid mixtures. *Chem. Sci.* **2017**, *8*, 6359−6374.
(16) Bruce, D. W.; Cabry, C. P.; Canongia Lopes, J. N.; Costen, M. L.; D'Andrea, L.; Grillo, I.; Marshall, B. C.; McKendrick, K. J.; Minton, T. K.; Purcell, S. M.; Rogers, S.; Slattery, J. M.; Shimizu, K.; Smoll, E.; Tesa-Serrate, M. A. Nanosegregation and Structuring in the Bulk and at the Surface of Ionic-Liquid Mixtures. *J. Phys. Chem. B* **2017**, *121*, 6002−6020.
(17) Cabry, C. P.; D'Andrea, L.; Shimizu, K.; Grillo, I.; Li, P.; Rogers, S.; Bruce, D. C.; Canongia Lopes, J. N.; Slattery, J. M. Exploring the bulk-phase structure of ionic liquid mixtures using small-angle neutron scattering. *Faraday Discuss.* **2018**, *206*, 265−289.
(18) Canongia Lopes, J. N.; Cordeiro, T. C.; Esperanca, J. M. S. S.; Guedes, H. J. R.; Huq, S.; Rebelo, L. P. N.; Seddon, K. R. Deviations from ideality in mixtures of two ionic liquids containing a common ion. *J. Phys. Chem. B* **2005**, *109*, 3519−3525.
(19) Castejón, H. J.; Lashock, R. J. Mixtures of ionic liquids with similar molar volumes form regular solutions and obey the cross-square rules for electrolyte mixtures. *J. Mol. Liq.* **2012**, *167*, 1−4.
(20) Cosby, T.; Kapoor, U.; Shah, J. K.; Sangoro, J. Mesoscale Organization and Dynamics in Binary Ionic Liquid Mixtures. *J. Phys. Chem. Lett.* **2019**, *10*, 6274−6280.
(21) Di Pietro, M. E.; Castiglione, F.; Mele, A. Anions as Dynamic Probes for Ionic Liquid Mixtures. *J. Phys. Chem. B* **2020**, *124*, 2879−2891.
(22) Costa, R.; Voroshylova, I. V.; Cordeiro, M. N. D. S.; Pereira, C. M.; Silva, A. F. Enhancement of differential double layer capacitance and charge accumulation by tuning the composition of ionic liquids mixtures. *Electrochim. Acta* **2018**, *261*, 214−220.
(23) Costa, R.; Pereira, C. M.; Fernando Silva, A. Structural ordering transitions in ionic liquids mixtures. *Electrochem. commun* **2015**, *57*, 10−13.
(24) Costa, R.; Pereira, C. M.; Silva, A. F. Role of the anion on the Interfacial Structure of Ionic Liquids Binary Mixtures at Mercury Interfaces. *Electrochim. Acta* **2016**, *195*, 150−157.
(25) Shin, S.; Greco, F.; Maier, F.; Steinrück, H. P. Enrichment effects of ionic liquid mixtures at polarized electrode interfaces monitored by potential screening. *Phys. Chem. Chem. Phys.* **2021**, *23*, 10756−10762.
(26) Navia, P.; Troncoso, J.; Romaní, L. Excess Magnitudes for Ionic Liquid Binary Mixtures with a Common Ion. *J. Chem. Eng. Data* **2007**, *52*, 1369−1374.
(27) Costa, R.; Pereira, C. M.; Silva, A. F. Charge storage on ionic liquid electric double layer: The role of the electrode material. *Electrochim. Acta* **2015**, *167*, 421−428.
(28) Voroshylova, I. V.; Ferreira, E. S. C.; Malcek, M.; Costa, R.; Pereira, C. M.; Cordeiro, M. N. D. S. Influence of the anion on the properties of ionic liquid mixtures: A molecular dynamics study. *Phys. Chem. Chem. Phys.* **2018**, *20*, 14899−14918.
(29) Buzzeo, M. C.; Hardacre, C.; Compton, R. G. Use of room temperature ionic liquids in gas sensor design. *Anal. Chem.* **2004**, *76*, 4583−4588.
(30) Toniolo, R.; Dossi, N.; Pizzariello, A.; Doherty, A. P.; Susmel, S.; Bontempelli, G. An oxygen amperometric gas sensor based on its electrocatalytic reduction in room temperature ionic liquids. *J. Electroanal. Chem.* **2012**, *670*, 23−29.
(31) AlNashef, I. M.; Leonard, M. L.; Kittle, M. C.; Matthews, M. A.; Weidner, J. W. Electrochemical generation of superoxide in room-temperature ionic liquids. *Electrochem. Solid-State Lett.* **2001**, *4*, 19−22.
(32) Lee, J.; Murugappan, K.; Arrigan, D. W. M.; Silvester, D. S. Oxygen reduction voltammetry on platinum macrodisk and screen-printed electrodes in ionic liquids: Reaction of the electrogenerated superoxide species with compounds used in the paste of Pt screen-printed electrodes? *Electrochim. Acta* **2013**, *101*, 158−168.
(33) Pozo-Gonzalo, C.; Howlett, P. C.; Hodgson, J. L.; Madsen, L. A.; MacFarlane, D. R.; Forsyth, M. Insights into the reversible oxygen reduction reaction in a series of phosphonium-based ionic liquids. *Phys. Chem. Chem. Phys.* **2014**, *16*, 25062−25070.
(34) Pozo-Gonzalo, C.; Torriero, A. A. J.; Forsyth, M.; MacFarlane, D. R.; Howlett, P. C. Redox Chemistry of the Superoxide Ion in a Phosphonium-Based Ionic Liquid in the Presence of Water. *J. Phys. Chem. Lett.* **2013**, *4*, 1834−1837.
(35) Hayyan, M.; Hashim, M. A.; Alnashef, I. M. Superoxide Ion: Generation and Chemical Implications. *Chem. Rev.* **2016**, *116*, 3029−3085.
(36) Atkin, R.; Borisenko, N.; Druschler, M.; El Abedin, S. Z.; Endres, F.; Hayes, R.; Huber, B.; Roling, B. An in situ STM/AFM and impedance spectroscopy study of the extremely pure 1-butyl-1-methylpyrrolidinium tris(pentafluoroethyl)trifluorophosphate/Au(111) interface: Potential dependent solvation layers and the herringbone reconstruction. *Phys. Chem. Chem. Phys.* **2011**, *13*, 6849−6857.
(37) Atkin, R.; Borisenko, N.; Druschler, M.; Endres, F.; Hayes, R.; Huber, B.; Roling, B. Structure and dynamics of the interfacial layer between ionic liquids and electrode materials. *J. Mol. Liq.* **2014**, *192*, 44−54.
(38) Doblinger, S.; Lee, J.; Silvester, D. S. Effect of Ionic Liquid Structure on the Oxygen Reduction Reaction under Humidified Conditions. *J. Phys. Chem. C* **2019**, *123*, 10727−10737.
(39) Islam, M. M.; Imase, T.; Okajima, T.; Takahashi, M.; Niikura, Y.; Kawashima, N.; Nakamura, Y.; Ohsaka, T. Stability of Superoxide Ion in Imidazolium Cation-Based Room-Temperature Ionic Liquids. *J. Phys. Chem. A* **2009**, *113*, 912−916.
(40) Nicholson, R. S. Theory and Application of Cyclic Voltammetry for Measurement of Electrode Reaction Kinetics. *Anal. Chem.* **1965**, *37*, 1351−1355.
(41) Paul, H. J.; Leddy, J. Direct Determination of the Transfer Coefficient from Cyclic Voltammetry: Isopoints as Diagnostics. *Anal. Chem.* **1995**, *67*, 1661−1668.
(42) Elgrishi, N.; Rountree, K. J.; McCarthy, B. D.; Rountree, E. S.; Eisenhart, T. T.; Dempsey, J. L. A Practical Beginner's Guide to Cyclic Voltammetry. *J. Chem. Educ.* **2018**, *95*, 197−206.
(43) Compton, R. G.; Banks, C. E. Electrode Kinetics. In *Understanding Voltammetry*, 3rd ed.; World Scientific: Hackensack, NJ, 2018; pp 37−82.
(44) Lee, J.; Du Plessis, G.; Arrigan, D. W. M.; Silvester, D. S. Towards improving the robustness of electrochemical gas sensors: Impact of PMMA addition on the sensing of oxygen in an ionic liquid. *Anal. Methods* **2015**, *7*, 7327−7335.
(45) Li, Q.; Jiang, J.; Li, G.; Zhao, W.; Zhao, X.; Mu, T. The electrochemical stability of ionic liquids and deep eutectic solvents. *Sci. China Chem.* **2016**, *59*, 571−577.
(46) Zhang, J.; Bond, A. M. Practical considerations associated with voltammetric studies in room temperature ionic liquids. *Analyst* **2005**, *130*, 1132−1147.
(47) Gancarz, P.; Zorębski, E.; Dzida, M. Influence of experimental conditions on the electrochemical window. Case study on bis-(trifluoromethylsulfonyl)imide-based ionic liquids. *Electrochem. commun* **2021**, *130*, 107107.
(48) Coustan, L.; Shul, G.; Bélanger, D. Electrochemical behavior of platinum, gold and glassy carbon electrodes in water-in-salt electrolyte. *Electrochem. commun* **2017**, *77*, 89−92.

https://doi.org/10.1021/acsphyschemau.2c00035
ACS Phys. Chem Au 2022, 2, 515−526

(49) Katayama, Y.; Onodera, H.; Yamagata, M.; Miura, T. Electrochemical Reduction of Oxygen in Some Hydrophobic Room-Temperature Molten Salt Systems. *J. Electrochem. Soc.* **2004**, *151*, A59.
(50) Rogers, E. I.; Huang, X. J.; Dickinson, E. J. F.; Hardacre, C.; Compton, R. G. Investigating the mechanism and electrode kinetics of the oxygenlsuperoxide (O2IO2-) couple in various room-temperature ionic liquids at gold and platinum electrodes in the temperature range 298−318 K. *J. Phys. Chem. C* **2009**, *113*, 17811−17823.
(51) Evans, R. G.; Klymenko, O. V.; Saddoughi, S. A.; Hardacre, C.; Compton, R. G. Electroreduction of oxygen in a series of room temperature ionic liquids composed of group 15-centered cations and anions. *J. Phys. Chem. B* **2004**, *108*, 7878−7886.
(52) Bhattacharjee, A.; Luis, A.; Santos, J. H.; Lopes-de-Silva, J. A.; Freire, M. G.; Carvalho, P. J.; Coutinho, J. A. P. Thermophysical properties of sulfonium- and ammonium-based ionic liquids. *Fluid Phase Equilib.* **2014**, *381*, 36−45.
(53) Ferreira, E. S. C.; Pereira, C. M.; Cordeiro, M. N. D. S.; Dos Santos, D. J. V. A. Molecular Dynamics Study of the Gold/Ionic Liquids Interface. *J. Phys. Chem. B* **2015**, *119*, 9883−9892.
(54) Kamalakannan, S.; Prakash, M.; Al-Mogren, M. M.; Chambaud, G.; Hochlaf, M. Alkyl Methyl Imidazolium-Based Ionic Liquids at the Au(111) Surface: Anions and Alkyl Chain Cations Induced Interfacial Effects. *J. Phys. Chem. C* **2019**, *123*, 15087−15098.
(55) Frontera, A.; Bauzá, A. Regium−π bonds: An Unexplored Link between Noble Metal Nanoparticles and Aromatic Surfaces. *Chem. - A Eur. J.* **2018**, *24*, 7228−7234.
(56) Gomes, C.; Costa, R.; Pereira, C. M.; Silva, A. F. The electrical double layer at the ionic liquid/Au and Pt electrode interface. *RSC Adv.* **2014**, *4*, 28914−28921.
(57) Uhl, B.; Cremer, T.; Roos, M.; Maier, F.; Steinruck, H. P.; Behm, R. J. At the ionic liquid|metal interface: Structure formation and temperature dependent behavior of an ionic liquid adlayer on Au(111). *Phys. Chem. Chem. Phys.* **2013**, *15*, 17295−17302.
(58) Cremer, T.; Stark, M.; Deyko, A.; Steinruck, H. P.; Maier, F. Liquid/Solid Interface of Ultrathin Ionic Liquid Films: [C 1 C 1 Im][Tf 2 N] and [C 8 C 1 Im][Tf 2 N] on Au (111). *Langmuir* **2011**, *27*, 3662−3671.
(59) Atkin, R.; El Abedin, S. Z.; Hayes, R.; Gasparotto, L. H. S.; Borisenko, N.; Endres, F. AFM and STM studies on the surface interaction of [BMP]TFSA and [EMIm]TFSA ionic liquids with Au(111). *J. Phys. Chem. C* **2009**, *113*, 13266−13272.
(60) Edwards, P. P.; Gray, H. B.; Lodge, M. T. J.; Williams, R. J. P. Electron transfer and electronic conduction through an intervening medium. *Angew. Chemie - Int. Ed* **2008**, *47*, 6758−6765.
(61) Lee, J.; Caporale, C.; McKinley, A. J.; Fuller, R. O.; Silvester, D. S. Electrochemical Properties of a Verdazyl Radical in Room Temperature Ionic Liquids. *Aust. J. Chem.* **2020**, *73*, 1001−1009.
(62) Silvester, D. S.; Uprety, S.; Wright, P. J.; Massi, M.; Stagni, S.; Muzzioli, S. Redox Properties of a Rhenium Tetrazolato Complex in Room Temperature Ionic Liquids: Assessing the Applicability of the Stokes-Einstein Equation for a Metal Complex in Ionic Liquids. *J. Phys. Chem. C* **2012**, *116*, 7327−7333.
(63) Bentley, C. L.; Li, J.; Bond, A. M.; Zhang, J. Mass-transport and heterogeneous electron-transfer kinetics associated with the ferrocene/ferrocenium process in ionic liquids. *J. Phys. Chem. C* **2016**, *120*, 16516−16525.
(64) De Vreese, P.; Haerens, K.; Matthijs, E.; Binnemans, K. Redox reference systems in ionic liquids. *Electrochim. Acta* **2012**, *76*, 242−248.
(65) Zhang, Y.; Rutland, M. W.; Luo, J.; Atkin, R.; Li, H. Potential-Dependent Superlubricity of Ionic Liquids on a Graphite Surface. *J. Phys. Chem. C* **2021**, *125*, 3940−3947.
(66) Kislenko, S. A.; Samoylov, I. S.; Amirov, R. H. Molecular dynamics simulation of the electrochemical interface between a graphite surface and the ionic liquid [BMIM][PF6]. *Phys. Chem. Chem. Phys.* **2009**, *11*, 5584−5590.
(67) Baldelli, S. Surface structure at the ionic liquid-electrified metal interface. *Acc. Chem. Res.* **2008**, *41*, 421−431.
(68) Bazant, M. Z.; Storey, B. D.; Kornyshev, A. A. Double layer in ionic liquids: Overscreening versus crowding. *Phys. Rev. Lett.* **2011**, *106*, 6−9.
(69) Shimizu, K.; Tariq, M.; Rebelo, L. P. N.; Lopes, J. N. C. Binary mixtures of ionic liquids with a common ion revisited: A molecular dynamics simulation study. *J. Mol. Liq.* **2010**, *153*, 52−56.

https://doi.org/10.1021/acsphyschemau.2c00035
ACS Phys. Chem Au 2022, 2, 515−526